An Interplay Between Infrared Multiphoton Dissociation Fourier-Transform Ion Cyclotron Resonance Mass Spectrometry and Density Functional Theory Computations in the Characterization of a Tripodal Quinolin-8-Olate Gd(III) Complex

Margherita De Bonis, Giuliana Bianco, Mario Amati, Sandra Belviso, Tommaso

Journal of The American Society for Mass Spectrometry
The official journal of The American Society for Mass Spectrometry

ISSN 1044-0305
Volume 24
Number 4

J. Am. Soc. Mass Spectrom. (2013) 24:589-601
DOI 10.1007/s13361-012-0570-0

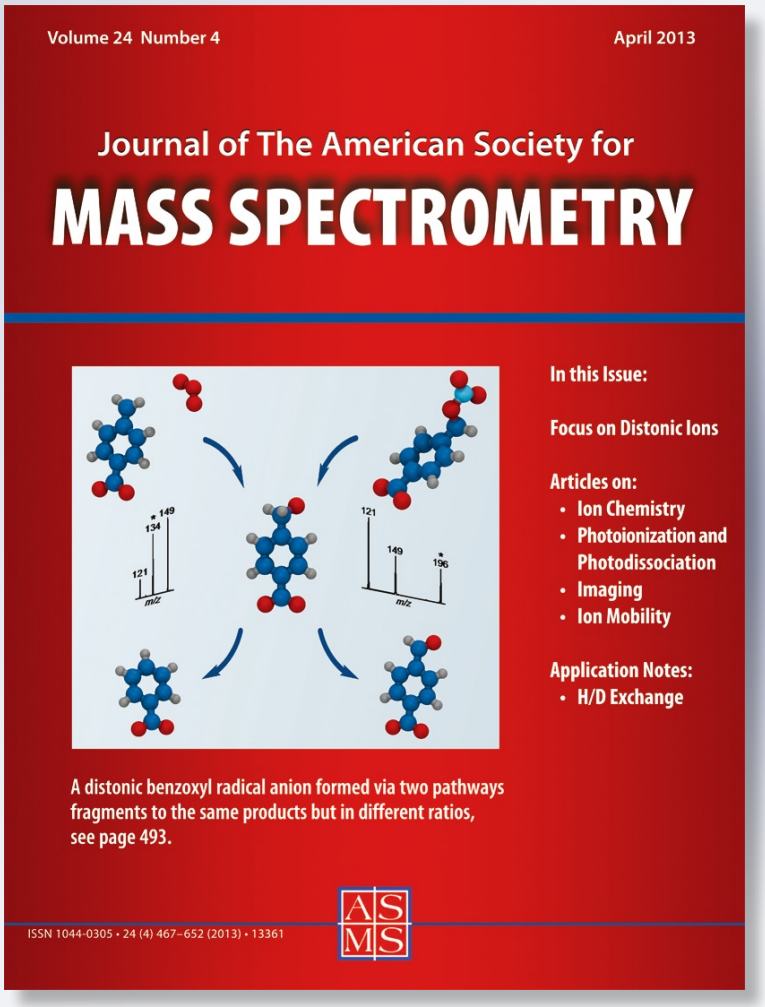

Springer

J. Am. Soc. Mass Spectrom. (2013) 24:589–601
DOI: 10.1007/s13361-012-0570-0

RESEARCH ARTICLE

An Interplay Between Infrared Multiphoton Dissociation Fourier-Transform Ion Cyclotron Resonance Mass Spectrometry and Density Functional Theory Computations in the Characterization of a Tripodal Quinolin-8-Olate Gd(III) Complex

Margherita De Bonis,[1,2] Giuliana Bianco,[2,4] Mario Amati,[1,2,5] Sandra Belviso,[1,2,5] Tommaso R. I. Cataldi,[3,6] Francesco Lelj[5]

[1]LaMI, Dipartimento di Scienze, Università degli Studi della Basilicata, Via dell'Ateneo Lucano, 10, 85100 Potenza, Italy
[2]Dipartimento di Scienze, Università degli Studi della Basilicata, Via dell'Ateneo Lucano, 10, 85100 Potenza, Italy
[3]Dipartimento di Chimica, Università degli Studi di Bari Aldo Moro, Campus Universitario, Via Orabona 4, 70126 Bari, Italy
[4]Centro Interdipartimentale CIGAS, Università degli Studi della Basilicata, Via dell'Ateneo Lucano, 10, 85100 Potenza, Italy
[5]LaSCAMM, INSTM- Sezione Basilicata, Università degli Studi della Basilicata, Via dell'Ateneo Lucano, 10, 85100 Potenza, Italy
[6]Centro Interdipartimentale SMART, Università degli Studi di Bari Aldo Moro, Campus Universitario, Via E. Orabona 4, 70126 Bari, Italy

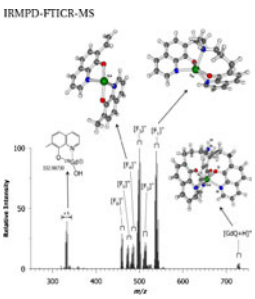

Abstract. A new hexadentate, tripodal 8-hydroxyquinoline based ligand (QH_3) and its gadolinium(III) *tris*-chelated (GdQ) complex with hemicage structure was investigated by using high resolution Fourier-transform ion cyclotron resonance mass spectrometry (FTICRMS). The protonated adduct of the free ligand and its hemicage tripodal Gd(III) complex, $[GdQ + H]^+$, were first observed in experiments of electrospray ionization (ESI) with a linear ion trap (LTQ) mass spectrometer and further investigated by using high resolution FTICRMS. Gas-phase dissociation of the protonated Gd(III) complex, by infrared multiphoton dissociation (IRMPD) FTICR MS, demonstrated a fragmentation pattern with six main product cluster ions labeled as $[F_n]^+$ (n=1 up to 6). These product ions suggest the elimination of 7-amino-alkyl or 7-alkyl chains of the hemicage moiety. High resolution MS conditions allowed the elucidation of the fragmentation pattern and product ion structures along with the determination, among the isotopic pattern of Gd, of the chemical compositions of closely related species, which differ in terms of hydrogen content. Among the Gd six naturally stable isotopes, ^{158}Gd is the most abundant, and its peak within each cluster was used as a reference for distinguishing each product ions. Computational DFT investigations were applied to give support to some hypothesis of fragmentation pathways, which could not have been easily justified on the basis of the experimental work. Furthermore, computational studies suggested the coordination geometry of the protonated parent complex and the five- and four-coordinated complexes, which derive from its fragmentation. Furthermore, experimental and computational evidences were collected about the octet spin state of the parent compound.

Key words: Infrared multiphoton dissociation, Ion cyclotron resonance, ICR, IRMPD, Gadolinum, Tripodal complex, Density functional study, DFT, Fragmentation pathways

Received: 19 October 2012/Revised: 7 December 2012/Accepted: 18 December 2012/Published online: 23 February 2013

Introduction

In recent years, electrospray ionization Fourier-transform ion cyclotron resonance mass spectrometry (ESI-FTICRMS) has become a very powerful tool for the characterization of many organometallic systems [1] ranging from transition metals to lanthanide complexes [2–4]. The lanthanide (III) sandwich complexes ML_2 (L = substituted phthalocyaninate ligand; M = europium, gadolinium) have been characterized by using ESI MS [5]. A number of Gd(III) complexes play a relevant role as paramagnetic contrast agents in the magnetic resonance imaging technique [6] and are continuously developed to achieve a more efficient and/or more specific imaging enhancement [7].

Electronic supplementary material The online version of this article (doi:10.1007/s13361-012-0570-0) contains supplementary material, which is available to authorized users.

Correspondence to: Francesco Lelj; *e-mail:* francesco.lelj@unibas.it, Tommaso R. I. Cataldi; *e-mail:* tommaso.cataldi@uniba.it

Among the complexating agents, 8-hydroxyquinoline (8HQ) is well known for its chelating ability, considered second only to ethylenediaminetetraacetic acid [8]. In fact, its conjugated basis quinolin-8-olate, acting as a bidentate ligand, effectively binds metal cations producing coordination compounds, which normally show high fluorescence quantum yields [9–14] in spite of the low fluorescence of the free 8HQ ligand [15, 16]. Strong fluorescence is one of the desirable properties of its complexes allowing fruitful applications in the field of organic light emitting diodes [17–19]. Recent studies have further suggested that quinolin-8-olate-based lanthanide complexes are good candidates for the design of near infrared emitting luminescent probes for biomedical applications due to their good stability, low toxicity, sizeable quantum yields in water, long excitation wavelength, and ability to interact with proteins as well [20]. A way for further enhancing the already large coordinating ability of quinolin-8-olate is to incorporate several quinolin-8-olate units in a tripodal or tetrapodal ligand functionalized with sulfonate groups, thus ensuring water solubility [21].

Reported herein are the results concerning the characterization of a novel tripodal quinolin-8-olate gadolinium complex (Figure 1) and its free ligand by electrospray ionization and tandem mass spectrometry (ESI-MS/MS) using FTICRMS and infrared multiphoton dissociation (IRMPD). Apparently, the tripodal ligand (QH_3) is able to arrange its donor atoms around the Gd(III) central metal (GdQ) to form a hemicage complex. In its protonated form (reported in Figure 1), because of the strong chelating effect of the 8HQ moieties, it is supposed to be a hexadentate ligand with the amine nitrogen atom interested by protonation.

The key to the structural identification and characterization of new coordination compounds, along with accurate mass measurements of protonated adducts, lies at the fragmentation capability offered by tandem MS systems. Their choice is largely determined by the pertinent features of the mass analyzer. FTICR mass spectrometry offers high resolving power and high mass accuracy [22, 23]. The fragmentation of the precursor ions isolated within the FTICR trapping cell can be induced by sustained off-resonance irradiation collision-induced dissociation (SORI-CID) [24], infrared multiphoton dissociation (IRMPD) [25, 26], blackbody infrared radiative dissociation (BIRD) [27, 28], surface-induced dissociation (SID) [29, 30], electron capture dissociation (ECD) [31] and electron transfer dissociation (ETD) [32]. To a great extent, the photo-fragmentation behavior of IRMPD is almost similar to the CID of selected ions whereby dissociation occurs by low-energy pathways. Yet IRMPD is preferred over CID because no collision gas is introduced into the ICR cell, and this facilitates accurate mass identification and streamlining product ion assignment with the high-resolution FTICR MS. A further and important advantage of IRMPD is that, being a non-resonant activation method [33], the precursor and ensuing neutral labile losses and ionic products are activated by IR irradiation in gas phase. These processes give rise to secondary and higher order fragments which can provide additional structural information compared to those obtained in a single resonant collision activation experiment [34–37]. Recently, Bianco et al. [38] have successfully employed IRMPD with high-resolution FTICR MS for a correct interpretation of anomalous fragments originated by a scrambling mechanism of peptides.

The combination of these experiments with Density Functional Theory (DFT) computations provided further insights about the preferred fragmentation pathways. Such study was based on the energy evaluation of different structures which are compatible with the composition of the observed fragments. Thus, relative ion energies were used as the main guide for justifying the relative abundances of the different observed product ions and hint possible fragmentation paths. Furthermore, DFT computations were applied for predicting the coordination geometry of the observed product ions and the preferred binding site of the proton in $[GdQ + H]^+$. An experimental evaluation of the structurally similar *tris*(quinolin-8-olato) Gd(III) (Gdq3) complex ground state spin multiplicity was performed to check if even in this kind of molecules the most stable electronic spin state corresponds to the octet one and to compare it with the computed one.

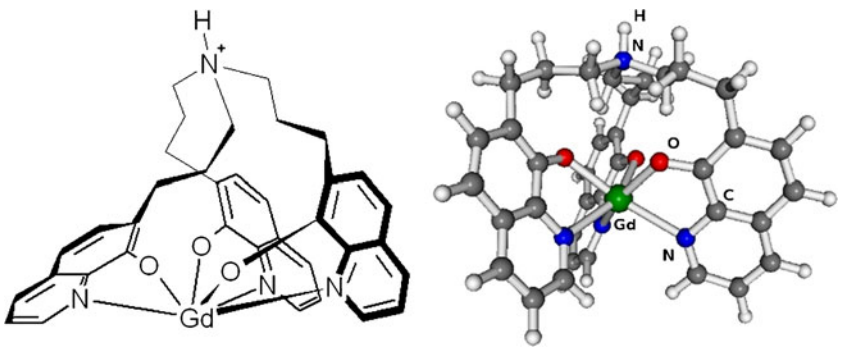

Figure 1. Tripodal quinolin-8-olate Gd(III) complex in its protonated form, $[GdQ + H]^+$ (the object of this investigation). The structure on the right was computed by methods stated in the following (see Electronic Supplementary Material, Computational Data Section, Table S-10)

Experimental and Methods

Chemicals

Analytical grade methanol was purchased from Sigma-Aldrich (Buchs, Switzerland). Stock solutions of the analytes were prepared by dissolving synthetic tripodalGd-complex in MeOH at a concentration of 1 μg/mL prior to infusion into the mass spectrometer. Dimethylsulfoxide-d_6 and cyclohexane used for ^{1}HNMR experiments were purchased from Sigma-Aldrich.

FTICR-MS and IRMPD FTICR-MS/MS

Accurate mass experiments were performed by using a LTQ-FT hybrid linear ion trap/7-T FTICR mass spectrometer (Thermo Fisher Scientific, Bremen, Germany) already described [39]. Positive ion ESI-MS was chosen for the detection of both the free ligand and the Gd(III) hemicage complex. Samples were directly infused into the source with a syringe pump at a flow rate of 5 μL/min. The spray voltage was set at 4 kV and the capillary temperature at 350 °C unless otherwise indicated. The MS detector was automatically tuned on the base peak, which optimized the remaining parameters. The used sheath gas (N_2) flow rate was five (arbitrary units) and the auxiliary gas was set to zero (arbitrary units). Full scan experiments were performed in the ICR cell in the range *m/z* 150–1000. Masses were acquired as profile data at a resolving power (RP) of 100,000 (RP = (*m/z*)/FWHM, full width at half maximum) at *m/z* 400. The automatic gain control (AGC) ion population target in full scan MS was 5,000,000 for FTICR MS. The maximum ion injection time was 200 ms for FTICR. Precursor ions were isolated in the linear ion trap and transferred into the ICR cell. The laser source with a nominal power output of 20 W in continuous mode is mounted downstream of the FTICR cell, vertically on the back of the magnet and shines into the ICR cell. In the upper part of the electronics cabinet at the rear side of the instrument, a mirror unit deflects the laser beam into the magnet bore through a ZnSe coated lens, which is highly permissible to infrared radiation. IRMPD with pulses of different time length (i.e., from 100 ms up to 250 ms, at a laser power of 100 arbitrary units was applied (Synrad, 20 W, 10.6 μm). The ion trap and FTICR mass spectrometer were calibrated according to manufacturer's instructions by using a solution of caffeine (*m/z* 195), MRFA (*m/z* 524), and Ultramark mix (*m/z* 1122, 1222, 1322, 1422, 1522, 1622, 1722, and 1822). Xcalibur software package (ver. 2.0 SR1 Thermo Fisher Scientific) was used for data acquisition, analysis and monoisotopic exact mass calculation. The mass spectrometric raw data were imported, elaborated, and plotted by SigmaPlot 9.0 (Systat Software, Inc., London, UK).

Computational Methods

Geometry optimizations were performed by density functional theory (DFT) computations with the recent meta-hybrid xc functional known as M06 [40] as implemented in the Gaussian09 suite of programs [41] and the 6-31 G basis set [42–46] for H, C, N, and O atoms. Some control calculations were also performed adding *d* polarization functions (6-31 G* basis set) for the same atom types. The Stuttgart/Dresden ECP basis set [47] and pseudopotential (SDD) for small core including relativistic effects was used for Gd. Default gradient and displacement thresholds were applied for the geometry optimization convergence criteria. Hard to converge (by conventional procedures) SCF computations in the case of open shell multiplets have been circumvented by using the quadratic convergent techniques [48]. The MOLEKEL 4.3 program [49, 50] has been used to draw some molecular structures besides chemical structures were drawn by ChemDraw Pro 8.0.3 (Cambridge Soft Corporation, Cambridge, MA, USA).

Synthesis of tris(Quinolin-8-olate)Gadolinium (Gdq_3)

A Gd(III) acetate aqueous solution was added dropwise to a 8-hydroxyquinoline (8q) methanol solution in a 1:3 Gd^{3+}/8q molar ratio. Upon addition, a yellow mixture was obtained. Subsequent dropwise addition of $Na_2CO_{3(}aq_{)}$ (0.6 M) till pH 8 determined the appearance of a plenty of precipitate. The latter was collected by filtration and washed with cold methanol. ESI-MS: *m/z* 591.06648 $[M + H]^+$ (exact *m/z* 591.06619); 446.01416 $[M\text{-}q]^+$ (exact *m/z* 446.01398).

Synthesis of Tripodal Quinolin-8-Olate Gadolinium Hemicage Complex (GdQ)

The ethanol solution of $Gd(OAc)_3$ hydrate salt was added dropwise to an ethanol solution of the ligand (synthetic details will be described elsewhere [51]) in a 1:1 ratio al 80 °C. The solution turned cloudy after the addition of the metal cation and few drops of triethylamine were added to complete the precipitation. After refluxing overnight, the total volume was reduced on a rotary evaporator and a yellow solid was filtered and washed with methanol [52].

Magnetic Susceptibility Measurements

The magnetic susceptibility was determined by ^{1}H NMR analysis through the Evans' method [53, 54]. The ^{1}H NMR spectra were collected with a 400 MHz (INOVA Varian, Palo Alto, California) spectrometer. In the inner space of a coaxial NMR tube, dimethylsulfoxide-d_6 (DMSO-d_6) with 0.2 % of cyclohexane was added and a sample solution (concentrations 8–10 mM) in the same mixture was put in the outer space. The measurements were performed on different sample solutions and were repeated at different temperatures to verify the Curie's law. The average resulting paramagnetic contribution to the molar susceptibility (χ_M^{para}) was not corrected by the tabulated diamagnetic factors being such correction negligible in this case [55].

Results

IRMPD-FTICR MS of the QH_3 Hemicage Ligand

Reported herein are results concerning the characterization of the QH_3 hemicage-coordination ligand (free ligand) by ESI-FTICR MS and tandem mass spectrometry (MS/MS) performed by IRMPD. The protonated adduct $[QH_3 + H]^+$ was observed at *m/z* 573.28601 (error −0.02 ppm) along with two isotopic peaks at *m/z* 574.28949 and 575.29297 (see Electronic Supplementary Material, Figure S-1a). No evidence was found for solvent adducts. By using the difference in their exact masses from the monoisotopic peak, the isotopic peaks were assigned to $^{13}C_1C_{35}H_{37}N_4O_3$ (exact *m/z* 574.28937, error 0.2 ppm) and $^{13}C_2C_{34}H_{37}N_4O_3$ (exact *m/z* 575.29273, error 0.4 ppm), respectively. The relative abundance of both isotope peaks due to the number of ^{13}C-atoms was evaluated; in agreement with Weber et al. [56], the accuracy of relative isotopic abundance measurement was not lower than 8 % in terms of deviation between experimental and theoretical abundance values. The observed peak positions were in good agreement with those of the simulated spectra (Table 1).

The $[QH_3 + H]^+$ precursor ion was photon irradiated for 150 ms at 100 % of power by an in-built 20 W continuous CO_2 laser source at a wavelength of 10.6 μm and the relevant IRMPD FTICR MS spectrum is reported in Figure S-1b (ESM). The photon induced fragmentation predominantly generated two ions at *m/z* 388.20206 and 186.09134 labeled as $[Q_1]^+$ and $[Q_2]^+$, respectively. The $[Q_1]^+$ ion is likely formed from the loss of a neutral 7-propenyl-8-hydroxyquinoline moiety, the latter being present at *m/z* 186.09129 as a protonated adduct. Table 1 summarizes the high resolution *m/z* data of the protonated QH_3 and its product ions upon IRMPD.

IRMPD FTICR MS of the Tripodal Gd(III) complex (GdQ)

As expected, the ESI mass spectrum of tripodal GdQ in the form of protonated adduct ($[GdQ + H]^+$) exhibits an ion cluster in the region from *m/z* 724 to 731 (Figure 2a). The occurrence of Gd(III) as a poly-isotopic element in the tripodal complex gives rise to an isotopologue cluster of the protonated adduct. The isotopic patterns of organometallic and coordination ions are often significantly more complex than those of the typical organic ones.

About forty chemical elements that do not frequently occur in organic compounds exist as polyisotopic elements [57–59]. For example, Dy, Gd, Hg, Mo, Nd, Ru, Sm, Sn, Te, Xe, and Yb have seven or more natural isotopes. Naturally occurring Gd is composed of six stable isotopes, (i.e., ^{154}Gd, ^{155}Gd, ^{156}Gd, ^{157}Gd, ^{158}Gd, and ^{160}Gd), and one radioisotope (^{152}Gd); ^{158}Gd and ^{160}Gd are the most abundant ones, with natural abundances of 24.84 % and 21.86 %, respectively [60]. The $[GdQ + H]^+$ ion cluster consists of eight peaks of not negligible intensity due to the presence of Gd in

Table 1. High-resolution MS data of the protonated QH_3 hemicage coordination ligand investigated by ESI-FTICR MS and IRMPD-FTICR MS[a]

Ion identity	Chemical formula	Measured *m/z* value[b]	Exact mass[c]	mmu[d]	ppm[e]	$[M+1]^+$ [f]	Relative intensity (%)[g]	$[M+2]^+$[h]	Relative intensity (%)[g]
$[QH_3+H]^+$	$[C_{36}H_{37}N_4O_3]^+$	573.28601	573.28602	−0.01	−0.02	574.28949	36.4 (38.94)	575.29297	6.3 (7.37)[g]
$[Q_1]^+$	$[C_{24}H_{26}N_3O_2]^+$	388.20206	388.20195	0.11	0.28	389.20590	24.8 (25.96)	390.20923	2.7 (2.40)[g]
$[Q_2]^+$	$[C_{12}H_{12}NO]^+$	186.09129	186.09134	−0.05	−0.26	187.09474	9.0 (12.98)	188.09811	0.5 (0.21)[f]

[a]See the experimental conditions described in the Fig. S-1 caption (see ESM).
[b]Experimental value of positively charged molecules.
[c]Monoisotopic exact mass was calculated by using the Xcalibur software package (ver. 2.0; Thermo Fisher Scientific).
[d]Mass error in millimass units: (accurate mass − exact mass)×1000.
[e]Error expressed in parts per million (ppm) and evaluated as $10^6\times$ (accurate mass − exact mass)/exact mass.
[f]Experimental values of the $[M+1]^+$ isotopic peak having a single ^{13}C.
[g]Relative intensity of the isotopic peaks $[M+1]^+$ and $[M+2]^+$; values in parenthesis are the expected relative abundances based on the presence of one ^{13}C and two ^{13}C isotopes, respectively.
[h]Experimental values of the $[M+2]^+$ isotopic peak.

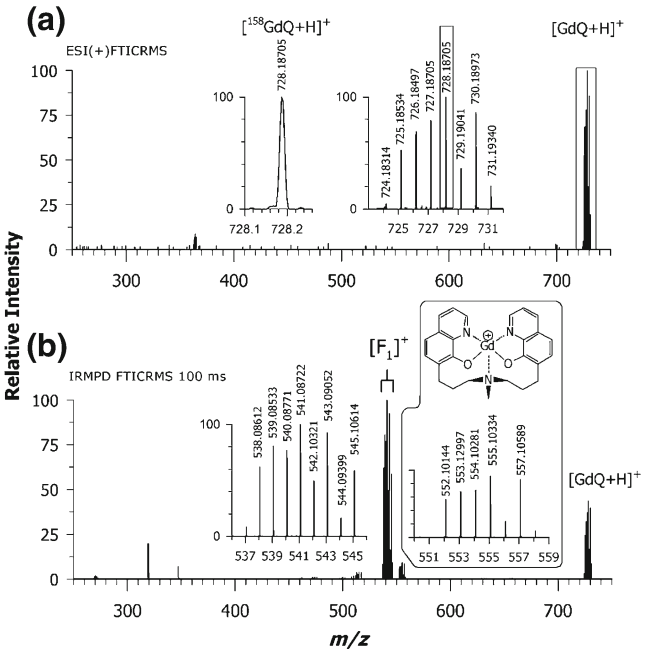

Figure 2. **(a)** High resolution mass spectrum by ESI-FTICRMS of the protonated form of GdQ, which is labeled as $[GdQ + H]^+$; **(b)** Product ion spectrum obtained by IRMPD FTICR MS of the $[GdQ + H]^+$ ion. The isolation width was *m/z* 10 with an automatic gain control target value of 5×10^6, maximum fill 200 ms. After transfer to the ICR cell, precursor ion populations were photon-irradiated for 100 ms at 100 % laser power (CO_2, 20 W). Each IRMPD scan was acquired as an FTICR MS/MS spectrum ($150<m/z<1000$) with mass resolving power of 100,000 FWHM at *m/z* 400. Each displayed spectrum represents the sum of at least 10 scans. Enlarged views of isotope patterns are shown in inset of plots **(a)** and **(b)**. The suggested product ion at *m/z* 555.1 is reported in inset **(b)**. See accurate MS data summarized in Table S-1

the complex structure with the most abundant ion at *m/z* 728.18705 (see inset in Figure 2a), which corresponds to the ^{158}Gd isotopologue. The FTICRMS instrument allowed to distinguish all the isotopologues and to assign the chemical composition to each signal. In detail, the eight signals corresponding to the six most abundant isotopes of Gd (i.e., ^{154}Gd (at *m/z* 724.18314), ^{155}Gd (at *m/z* 725.18534), ^{156}Gd (at *m/z* 726.18497), ^{157}Gd (at *m/z* 727.18705), ^{158}Gd (at *m/z* 728.18705), and ^{160}Gd (at *m/z* 730.18973) and two additional signals originating from the simultaneous presence of one ^{13}C and one ^{158}Gd (at *m/z* 729.19041) and one ^{13}C atom and one ^{160}Gd (at *m/z* 731.19340), respectively. The accurate mass data are listed in Table S-1 (Electronic Supplementary Material).

The fragmentation behavior of $[GdQ + H]^+$was examined by IRMPD FTICR MS under the high-vacuum conditions of the trapping cell. The slow heating IRMPD tool provides a tunable irradiation time length which can be employed to control the extent of secondary fragmentation and, consequently, to reach fragmentation pathways not available by single-pass CID external to the ICR cell [33]. Precursor ion isolation was performed with a relatively wide window of 10 *m/z*, which included all the eight main isotopologues ions: M–4, M–3, M–2, M–1, M+0, M+1, M+2, and M+3 in the *m/z* range 724–731. The product ion spectrum after photon irradiation for 100 ms at 100 % laser power is shown in Figure 2b. The IRMPD mass spectra were produced by a single charged precursor ion and yielded a major product cluster ion in the range *m/z* 537–545. More details of this cluster ion will be given in the next paragraph as it represents the overlapping of at least three closely related species. Note also the occurrence of a cluster ion at *m/z* 552–557 (see expanded view in Figure 2b), which seems to be the result of a direct C-C bond breaking with the neutral loss of 7-ethyl-8-hydroxyquinoline from the tripodal chelant and formation of a methyl tertiary amine; as described in the following, the suggested structure on a computational basis is displayed in inset of Figure 2b.

As the amount of energy deposition from a single IR photon of a CO_2 laser is about 0.1 eV, long irradiation times are needed for effective IRMPD. Therefore, an irradiation time of 250 ms was applied to obtain effective gas-phase fragmentation and the almost complete disappearance of the precursor ion signal. Six distinct product cluster ions, identified as F_1 trough F_6, in the regions *m/z* 535–544, *m/z* 509–517, *m/z* 494–503, *m/z* 483–489, *m/z* 470–476, and *m/z* 456–463 were observed, respectively (see Figure 3), along with a nearly complete depletion of the precursor ion (range *m/z* 724–731). It should be mentioned the occurrence of a low intensity ion cluster in the *m/z* 327–335 window, which could be the result of an extensive fragmentation of C–C, C–O, and donor–Gd bonds. As the isotopic cluster closely resembles that of positively charged Gd compounds and the most intense peak occurs at *m/z* 332.98730, we suggest the formation of a $[C_{10}H_9NO_2Gd]^+$ ion in which two quinoline-8-olate ligands have been lost from the precursor ion (a possible structure of such ion is illustrated in the inset of Figure 3). Interestingly, accurate mass data of such a ion, with a mass error of −1.3 ppm ($[C_{10}H_9NO_2{}^{158}Gd]^+$) was found, suggesting a very good mass accuracy.

The identification of the six clusters (F_1–F_6) was a difficult task because the spectra were further complicated by fragment ions having different hydrogen content (vide infra). When two hydrogen atoms are removed, the isotopic distribution is shifted to lower *m/z* by 2.01565 Da. Consequently, the two isotopologue distributions significantly overlap and it is quite tricky to determine which spectral signal corresponds to each particular species. Only the high mass accuracy and resolution allowed to unequivocally identifying each fragment.

For most of these ions, the achieved resolving power (i.e., greater than 100,000 FWHM) was of uppermost usefulness to resolve closely related peaks and to determine the charge states from the isotope spacing. Each peak in the X-th ion cluster F_X

was identified as $F_{X,Y}$, where Y is the peak number in the mass spectrum (see Table S-2, ESM). Here, the *m/z* signal cluster $[F_1]^+$ in the range *m/z* 535–547 is discussed (Figure 4).

Magnification of the isotopic cluster of this product ion highlights (see upper part of Figure 4) that each *m/z* signal is actually the result of at least two overlapping isotopologue clusters which differ in the number of hydrogen atoms. As summarized in Table S-2, three product ions can be associated to this cluster; they differ by one or two H_2 units and have been indicated as $[I_1]^+$, $[I_1\text{-}H_2]^+$ and $[I_1\text{-}2H_2]^+$. Scheme 1 (see below) collects the postulated structures of such ions.

Mass spectral identification of all the *m/z* signals was done on the basis of likely elemental composition estimated by accurate values. As an example, the product ion at *m/z* 543.10334 is associated to the $[C_{24}H_{23}N_3O_2{}^{158}Gd]^+$ molecular formula. It can be considered derived from the neutral loss of 7-propylen-8-hydroxiquinoline and it is hereafter denoted as $[F_{1.18}]^+$. As the exact mass of the $[C_{24}H_{23}N_3O_2{}^{158}Gd]^+$ ion is 543.10258, a good accuracy of 1.4 ppm (mmu = +0.76*m/z* units) was obtained. Additional and more abundant signals were observed at *m/z* 541.08744 (i.e., $[F_{1.12}]^+$) and 539.07201 (i.e., $[F_{1.6}]^+$), which correspond to species with a lower content of hydrogen, $[C_{24}H_{21}N_3O_2{}^{158}Gd]^+$ and $[C_{24}H_{19}N_3O_2{}^{158}Gd]^+$, respectively.

More dehydrogenated $[F_1]^+$ signals (i.e., $[I_1\text{-}H_2]^+$ along with $[F_{1.5}]^+$, $[F_{1.7}]^+$, $[F_{1.9}]^+$, $[F_{1.12}]^+$ and $[F_{1.17}]^+$) correspond to the five most abundant isotopes of Gd (i.e., ^{155}Gd (at *m/z* 538.08634), ^{156}Gd (at *m/z* 539.08538), ^{157}Gd (at *m/z* 540.08778), ^{158}Gd (at *m/z* 541.08744), and ^{160}Gd (at *m/z* 543.08997). Additional $[I_1\text{-}H_2]^+$ signals in the mass spectrum were due to the simultaneous presence of one ^{13}C and one ^{158}Gd ($[F_{1.15}]^+$at *m/z* 542.09037) and one ^{13}C plus one ^{160}Gd ($[F_{1.19}]^+$at *m/z* 544.09370). Moreover, ions having lost two hydrogen atoms, (i.e., $[I_1\text{-}2H_2]^+$ and peaks: $[F_{1.1}]^+$, $[F_{1.2}]^+$, $[F_{1.3}]^+$, $[F_{1.4}]^+$, $[F_{1.6}]^+$, and $[F_{1.11}]^+$) were observed and again correspond to the six most abundant Gd isotopes. The simultaneous presence of one ^{13}C and one ^{158}Gd ($[F_{1.8}]^+$ at *m/z* 540.07533), and one^{13}C with one^{160}Gd ($[F_{1.14}]^+$ at *m/z* 542.07791) was also detected for $[I_1\text{-}2H_2]^+$.

In the Electronic Supplementary Material, the interested reader can find a detailed list of all the resolved peaks belonging to the $[F_2]^+$, $[F_3]^+$, $[F_5]^+$, and $[F_6]^+$ clusters (see Figure S-4 and Table S-3, Figure S-5 and Table S-4, Figure S-6 and Table S-6, and Table S-7, respectively). The $[F_4]^+$ product ion cluster is discussed in details below. By comparing Figure. 2b and Figure 3, this ion cluster only appears when the irradiation time is long enough (250 ms) to allow gas-phase dissociation of the precursor ion with formation of a dominant species (vide infra) and consistent fragmentation of $[GdQ + H]^+$ (see Scheme 1). Figure 5 (bottom part) shows the IRMPD FTICR mass spectrum of the $[F_4]^+$ cluster; the enlarged views of the most intense peaks are depicted as well in the upper part of the same figure. The most intense signal was found at *m/z* 486.04435, assigned to $[C_{21}H_{16}N_2O_2{}^{158}Gd]^+$ and labeled as $[F_{4.6}]^+$. All the isotopologue ions containing the Gd isotopes are also

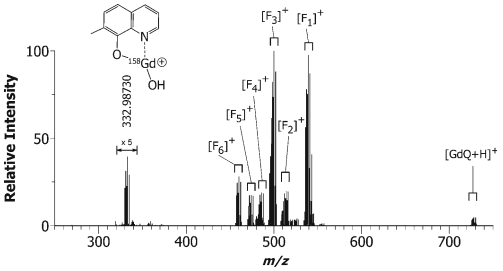

Figure 3. Product ion spectra obtained by IRMPD FTICR MS of the protonated Gd(III) complex $[GdQ + H]^+$; precursor ion populations were photon-irradiated for 250 ms at 100 % (20 W) laser power. Apart from the irradiation time, experimental conditions as reported in Figure 2 caption

present, and *m/z* data are summarized in Table S-5 ESM. Note that this product cluster ion exhibits a predominant species ($[C_{21}H_{16}N_2O_2Gd]^+$, labeled as $[I_4\text{-}H_2]^+$) plus a significantly less populated ion, which can be considered the hydrogenated form of the previous one ($[C_{21}H_{18}N_2O_2Gd]^+$, labeled as $[I_4]^+$). The $[I_4\text{-}H_2]^+$ and $[I_4]^+$ relative abundance is 100:6 (from peak relative intensities) as reported in Table S-8 ESM.

The occurrence of hydrogenated and dehydrogenated fragment ions was observed in the $[F_2]^+$ and $[F_3]^+$ clusters (see ESM for a detailed discussion about peak assignment in these clusters and Scheme 1 for the associated ion structures). These ions will be labeled as $[In]^+$ and $[In\text{-}H_2]^+$ (n=2 and 3) in the following. Note that the relative abundances of hydrogenated and dehydrogenated forms producing $[F_2]^+$ and $[F_3]^+$ are almost comparable. Indeed, the hydrogenated forms are predominant with similar relative populations, viz. 100:55 for $[I_2]^+$ versus $[I_2\text{-}H_2]^+$ and 100:48 for $[I_3]^+$ versus $[I_3\text{-}H_2]^+$. Conversely, as said above, the relative intensity of $[I_4]^+$ in comparison to $[I_4\text{-}H_2]^+$ is approximately 6:100 and represents an interesting point of discontinuity that was worthy of further investigation. This finding will be treated in the "Discussion" section below.

Structure of Ions and Isomer Stability: Inner Coordination Sphere

No indications of the starting geometry of the tripodal Gd(III) complex can be inferred from the mass data, although the parent complex must be a *fac* isomer due to constraints of the whole ligand structure [51]. Such a hypothesis has been confirmed by DFT computations which describes a hexadentate chelating behavior of the ligand in its protonated form (Figure 1). A possible seven-coordinated tautomer in which the nitrogen amine atom coordinates the central metal and the proton moved to one of the three oxygen atoms appears to be less stable by 27.06 kcal/mol (Figure S-7 and Table S-9). This suggests that the amine-

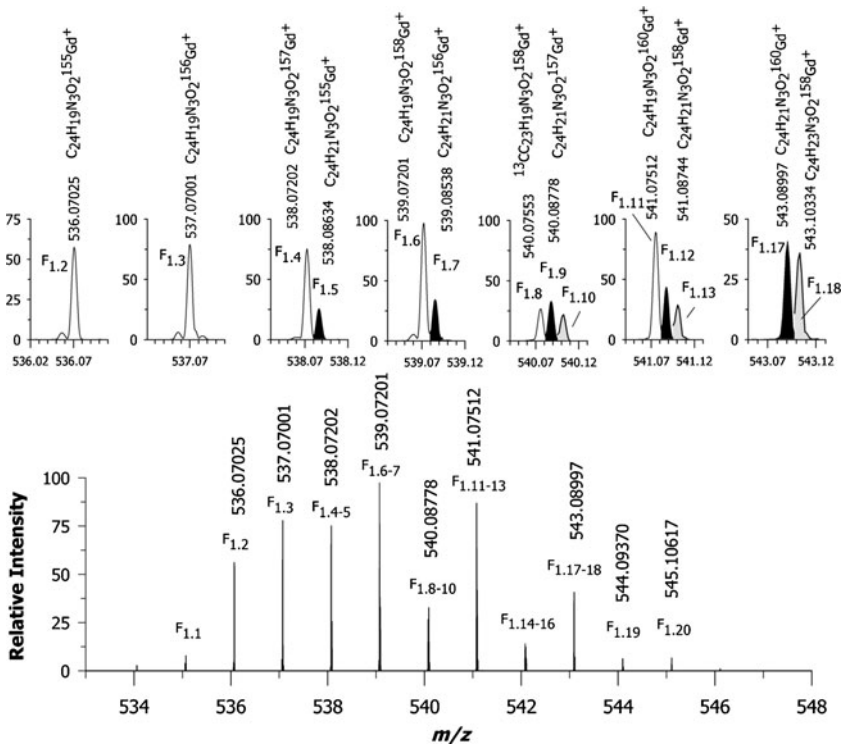

Figure 4. IRMPD FTICR mass spectrum of the product cluster ion labeled as $[F_1]^+$ in Figure 3. In the upper part, enlarged views of the most intense peaks are shown. The experimental conditions are the same detailed in Figure 3. Accurate mass data are listed in Table S-2 (ESM)

nitrogen protonated hexacoordinated Gd(III) complex is the precursor ion.

Owing to the mass indication that suggests a loss of a quinolin-8-olate moiety as a necessary step to produce the $[F_n]^+$ (n=1–6) clusters, the coordination sphere around the Gd^{3+} ion should contain only four donor atoms in $[F_n]^+$ (n=2–6) clusters but possibly a five-coordinated compounds in $[F_1]^+$ cluster ions. In the latter case, we applied DFT computational methods to determine the coordination number (and related coordination geometry) in the case of $[I_1]^+$ (Scheme 1). According to this study, $[I_1]^+$ is a five-coordinated complex in which the amine donor atom is coordinated to the central metal. The alternative four-coordinated geometry in which only the two quiniline-8-olate moieties are coordinated has been computed less stable by 3.70 kcal/mol (Figure S-9 and Table S-11). In this light, $[I_1]^+$ and, by extension, its dehydrogenated forms ($[I_1\text{-}H_2]^+$ and ($[I_1\text{-}2H_2]^+$) were reported as five-coordinated complexes in Scheme 1.

$[F_n]^+$ (n=2–6) clusters are surely associated to four-coordinated complexes. In this case, several possible coordination geometries can be postulated and DFT computations were applied to determine the most stable stereoisomers deriving from different quinoline-8-olate ligands arrangements around the central metal. In fact, the main goal of the performed computational study was to achieve suggestions about the preferred experimentally observed fragmentation pathways. In this light, a computational study that claims to give information about the energy-preferred fragmentation pathways cannot overlook the possibility of stereoisomers of different stability.

On the simple rationale that Gd(III) is an f^7 cation with a half-full shell electronic configuration and that the f electrons do not strongly influence the geometry of the coordination sphere, we assumed as a starting geometry a hypothetical tetrahedral structure according to the VSEPR model. This is the predicted geometry in the case of d^0, d^5, and d^{10} tetracoordinated transition metal complexes [61]. Computations indeed show that this simple rationale does not work and that possible interactions between the two quinoline-8-olate ligands largely modify the starting geometry. Figure 6a shows a schematic view of the three $[I_4]^+$ computed conformers. The relative stability of the different isomers has been investigated by using $[I_4]^+$ as a reference ion owing to the smaller number of atoms even preserving substituents on both the quinolin-8-olate ligands. As detailed in Figure 6b, the computed geometries are reminiscent of a distorted trigonal bipyramid with a missing equatorial ligand. This coordination geometry allows three diastereoisomeric structures which differ in the oxygen and/or nitrogen atoms arrangement within the inner coordination sphere. The above evoked combinations are: $O_{ax}N_{eq}$-$O_{ax}N_{eq}$, $O_{eq}N_{ax}$-$O_{eq}N_{ax}$, and $O_{eq}N_{ax}$-$O_{ax}N_{eq}$. According to the computations, the $O_{ax}N_{eq}$-$O_{ax}N_{eq}$ isomer is the most stable

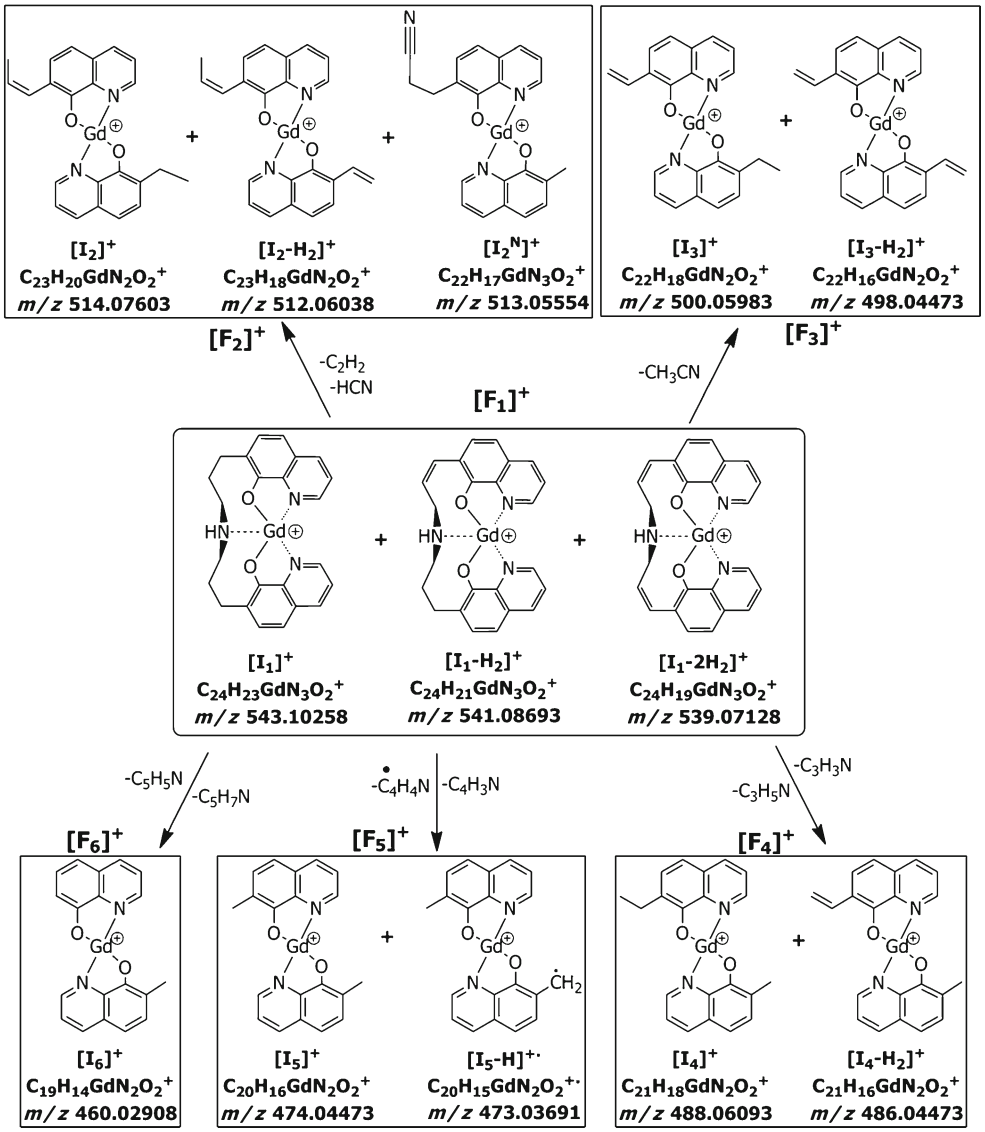

Scheme **1.** Observed ions and proposed fragmentation paths for the putative formation of product cluster ions from the $[F_1]^+$ ion under IRMPD of the tripodal $[GdQ + H]^+$ complex within the FTICR MS trapping cell. The exact *m/z* value of each product ion is given. The reported structures are not intended to give insights about the compound structures; they only give information about their composition

in energy. The computed N_{eq}-Gd-N_{eq} bond angle amounts to 89.80 degrees, the O_{ax}-Gd-O_{ax} to 147.26 degrees.

The energy trend $O_{ax}N_{eq}$-$O_{ax}N_{eq}$ < $O_{eq}N_{ax}$-$O_{eq}N_{ax}$ < $O_{eq}N_{ax}$-$O_{ax}N_{eq}$ is preserved in all the studied isomers of $[I_2]^+$ and $[I_3]^+$, according to our computations (for further details see Tables S-12 through S-19). This finding suggests that each product ion undergoes a significant rearrangement of the coordination sphere after losing one quinoline-8-olate ligand and the connected aliphatic chains. In fact, the loss of one quinolin-8-olate ligand from the precursor positive ion would lead to a structural conformation in which two oxygen donor atoms are in relative *cis* position. On the contrary, the preferred computed isomer seems to present the oxygen atoms in *trans* relative position (i.e., $O_{ax}N_{eq}$-$O_{ax}N_{eq}$, reminiscent of the $[I_1]^+$ cation (see Figure S-9a) whose rearrangement is probably due to the edge insertion of the amine nitrogen atom on the Gd cation between the two coordinated oxygen atoms after the loss of the quinoline-8-olate ligand and the connected aliphatic chains.

Spin Multiplicity of the Hemicage Tripodal Gd(III) Complex

The Gd(III) complexes might exist in different multiplicity states as the Gd^{3+} ion has an f^7 electronic configuration. As a primary choice in the performed computational study, the

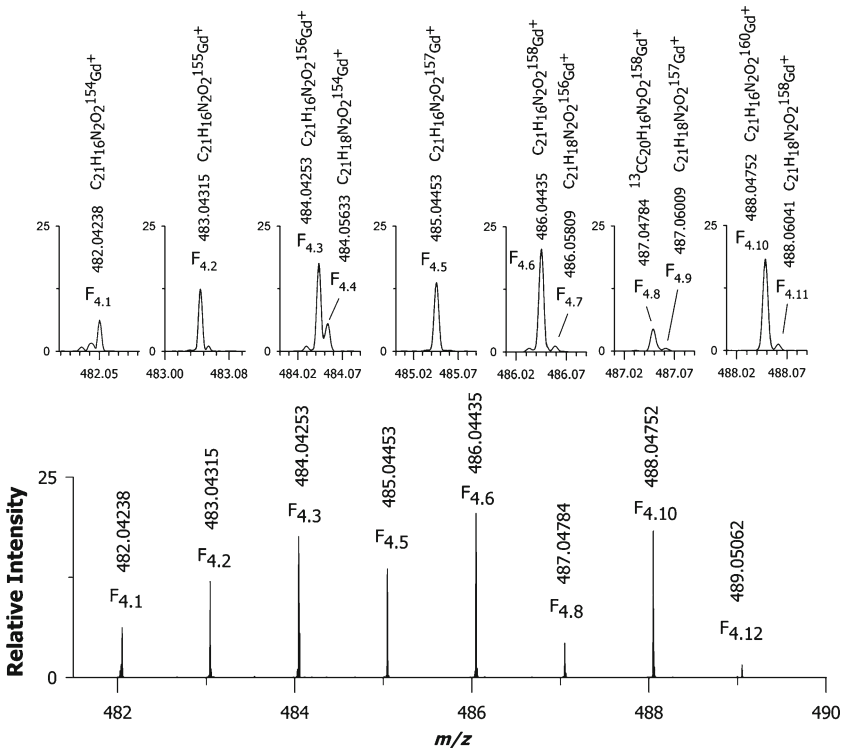

Figure 5. IRMPD FTICR mass spectrum of the $[F_4]^+$ product cluster ion obtained from the precursor ion $[GdQ + H]^+$. In the upper part are shown the enlarged view of the most intense peaks. See experimental conditions of the Figure 3 caption. Accurate mass data are listed in Table S-5 (ESM)

octet spin multiplicity has been imposed. In order to confirm that this choice leads to the ground state, we have computationally evaluated also the energies of the lower multiplicity states. As a reference compound, we used the $O_{ax}N_{eq}$-$O_{ax}N_{eq}$ isomer of the *bis*-(quinolin-8-olate) Gd(III) cation complex. That is, no substituents have been included in the quinoline-8-olate ligands so to reduce the computational effort without significantly perturbing the ligands influences on the central metal ion. Structure optimizations of the octet, sextet, quartet, and doublet spin states have been performed (see Figure S-10 and Table S-20 for details). In all the cases, small structural changes have been observed so that the $O_{ax}N_{eq}$-$O_{ax}N_{eq}$ conformation has been preserved. However, the energy trend is 0.00, +35.58, +126.00, and +165.59 kcal/mol for octet, sextet, quartet and doublet, respectively. The results indicate that, at unrestricted DFT level, the octet is the most stable spin state. Furthermore, the coordination environment of the complex marginally influences the f^7 Gd^{3+} electronic configuration, a fact that confirms the commonly accepted tendency of Gd^{3+} compounds to assume octet spin state.

In order to provide further experimental evidence, we have evaluated the spin multiplicity of the Gd^{3+} complexes by NMR spectrometry. Due to the poor solubility of the title compound (GdQ), the analysis was performed on the more soluble analogue *tris*-(quinolin-8-olate) Gadolinium, Gdq_3, whose synthesis has been detailed in the "Experimental and Methods" section [62]. The magnetic susceptibility of this compound was determined by ^1H NMR analysis through the Evans' method (see the Experimental and Methods sections). The measurements were performed in deuterated dimethylsulfoxide (DMSO-d_6) by measuring the proton resonance shift of cyclohexane that was incorporated in the

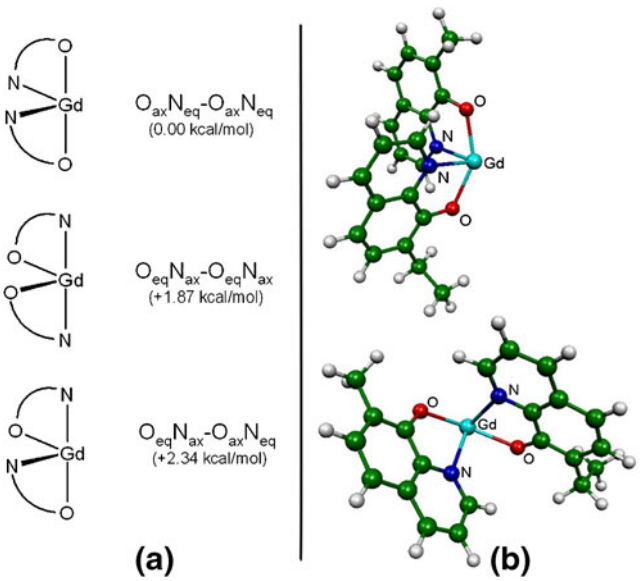

Figure 6. **(a)** A schematic view of the three $[I_4]^+$ computed conformers and their relative energy stability in parenthesis; **(b)** two more detailed sketches of the most stable in energy $O_{ax}N_{eq}$-$O_{ax}N_{eq}$ computed conformer structure

sample solution as inert reference compound. The resulting magnetic susceptibility was then related to the overall spin state of the substance and hence to the number of unpaired electrons [55, 63]. For Gdq_3 complex, it was found an average number of 6.35 unpaired electrons with a standard deviation of 0.01. This value can be considered in satisfactory agreement with the f^7 Gd^{3+} configuration already reported in literature and with our computations that showed that the fragment ions with octet multiplicity were the most stable ones.

Discussion

The fragmentation products by IRMPD of the protonated hemicage ligand $[QH_3 + H]^+$ shows two fragments whose mass is consistent with the dissociation processes reported in Scheme 2a (see also Table 1 and Figure S-1). The preferred fragmentation leads to a positively charged 7-propyl-8-hydroxyquinoline ligand and a neutral secondary amine (process *p*). It consists in a direct heterolytic N–C bond breaking of the amine function. Its higher kinetic rate is what can be expected on the basis of the associated smaller structural rearrangement of the reactive precursor in comparison of the slower process *s*. Obviously, the produced neutral amines could not be further investigated by mass spectrometry.

Scheme 2b depicts analogues fragmentation pathways for the hemicage tripodal $[GdQ+ H]^+$ complex. In this case, the 8-hydroxyquinoline moieties are deprotonated because the oxygen atoms coordinate the central metal, thus, process *p* would produce the shown zwitterionic compound (it can isomerize to form the sketched neutral 7-propenyl-8-hydroxyquinoline) plus the positively charged *bis*-chelated Gd complex that has been referred as $[I_1]^+$ in Scheme 1. As in the case of the free-ligand process *p*, such a fragmentation process is relatively fast and leads to the secondary amine that now is charged because of the presence of the cationic central metal. Hence, further fragmentation, if present, can be observed in this case.

$[GdQ + H]^+$ process *s* would lead to a negatively charged 7-propenylquinolin-8-olate plus a doubly positively charged complex ion ($[I_1']^{2+}$ in Scheme 2b), which was not experimentally observed. In this case, the slower process *s* fragmentation path (already discussed in the case of the free ligand) could be further hindered by the additional energy necessary to take apart ions of opposite charges. This could explain the lack of signals associated to hypothetical $[I_1']^{2+}$.

As detailed before, Figure 2b shows the fragmentation induced after a 100 ms irradiation time in IRMPD FTICR MS experiments. Note that the $[F_1]^+$ cluster is evident at about 538–545 *m/z* with a very low intensity cluster at 509–517 *m/z*, which has been labeled as $[F_2]^+$. After a longer irradiation time (250 ms), the fragmentation pattern is more complex (Figure 3). The $[F_n]^+$ clusters from n=2 to n=6 now are clearly present and the $[F_3]^+$ cluster produces the most intense signals. Such a change from shorter to longer irradiation times is suggestive of further photon-induced fragmentation from $[F_1]^+$ to lighter fragments. With the aim to support this idea, CID-based studies have been performed in tandem MS using the linear trap quadrupole (LTQ) mass analyzer. Fig. S-3b shows the ESI-MS/MS spectrum obtained by gas-phase fragmentation performed on the precursor ion at *m/z* 728. Interestingly the $[F_1]^+$ cluster was observed as the most predominant signal at a collision energy of 30 % (a.u.), in good agreement with experimental data observed in high resolution IRMPD FTICR MS. Upon consecutive CID, the resultant product ion spectrum (MS^3) of the $[F1]^+$ ion cluster engenders six main clusters (see Figure S-3c) with relative intensities which are comparable to the IRMPD ones after 250 ms laser irradiation (Figure 3). Conceivably, this experimental finding is consistent with a mechanism in which the product ions associated to $[F_1]^+$ (i.e., $[I_1]^+$, $[I_1\text{-}H_2]^+$ and $[I_1\text{-}2H_2]^+$) are indeed the precursor ions for all the other fragments as suggested by IRMPD FTICR MS experiments. Scheme 1 shows the fragmentation processes from $[F_1]^+$ plus a possible neutral loss in each process.

Further insights into the fragmentation pathways from the $[F_1]^+$ cluster can be obtained from the already discussed Table S-2 (ESM), which lists the relative abundances of hydrogenated and dehydrogenated forms of each fragment. As discussed above, $[F_2]^+$, $[F_3]^+$, and $[F_4]^+$ are associated to a couple of compounds which differ by a H_2 molecule. Such ionic species in each couple have been labeled as $[I_n]^+$ and $[I_n\text{-}H_2]^+$ in Scheme 1. $[I_2]^+$ and $[I_3]^+$ populations appear higher in comparison to the respective counterparts $[I_2\text{-}H_2]^+$ and $[I_3\text{-}H_2]^+$, whereas the $[I_4]^+$ population is very low in comparison to $[I_4\text{-}H_2]^+$. This anomaly has been further investigated by DFT computations.

A first hypothesis taken into account was the possibility that $[I_n\text{-}H_2]^+$ is originated from $[I_n]^+$ by H_2 elimination. Table 2A collects the computed reaction energies of these processes. As easily expected, the dehydrogenation processes are associated to very similar energy variations in the three studied cases. Although such a study can explain the higher population of $[I_2]^+$ and $[I_3]^+$ in comparison to their dehydrogenated forms, it is absolutely unable to explain the anomalous behavior of $[I_4]^+$. In addition, the energy gaps between hydrogenated and dehydrogenated forms seem too large to explain the simultaneous presence of both the species in the cases of $[F_2]^+$ and $[F_3]^+$ clusters. Hence, a different rationale is needed for explaining the experimental findings. Table 2B reports also some postulated fragmentation pathways, which take place from the $[F_1]^+$ cluster ions and lead to the observed lighter fragments in $[F_2]^+$, $[F_3]^+$, and $[F_4]^+$ clusters. Those processes were chosen as the most reasonable because they do not imply the breaking of double bonds and are associated to the smallest required structural rearrangements. On a purely computational basis, it is possible to consider a concurrent production of the couple of fragments $[I_2]^+$ versus $[I_2\text{-}H_2]^+$ and the couple $[I_3]^+$ versus $[I_3\text{-}H_2]^+$. That is, $[I_2]^+$ and $[I_3]^+$ are produced from the same

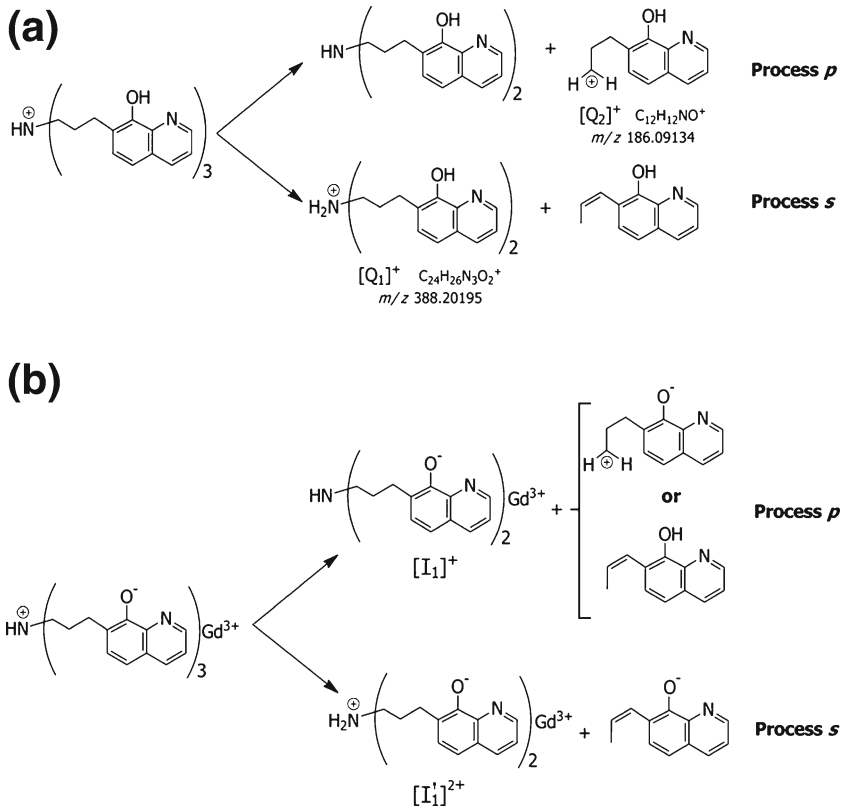

Scheme **2.** **(a)** Proposed fragmentation processes (***s*** and ***p***) of the protonated ligand $[QH_3 + H]^+$ with formation of two product ions: $[Q_1]^+$ and $[Q_2]^+$; **(b)** proposed fragmentation processes (*s* and *p*) of the tripodal quinolin-8-olateGd(III) complex as protonated adduct ($[GdQ + H]^+$) and formation of the $[I_1]^+$ ion (process *p*). The reported structures for of the $[I_1]^+$ and $[I_1']^+$ complexes are only indicative of the composition and are not intended to give information about the structure

precursor $[I_1\text{-}H_2]^+$, whereas both $[I_2\text{-}H_2]^+$ and $[I_3\text{-}H_2]^+$ are produced from $[I_1\text{-}2H_2]^+$. Furthermore, fragmentations toward $[I_2]^+$ and $[I_3]^+$ are energetically favored compared to fragmentations toward $[I_2\text{-}H_2]^+$ and $[I_3\text{-}H_2]^+$. In particular the reaction energy is ca. 1.2 kcal/mol more negative in both the $[I_n]^+$ than the $[I_n\text{-}H_2]^+$ counterpart. Moreover, in case of the $[F_3]^+$ cluster, the reaction energy is significantly more negative than $[F_2]^+$. In this light, it can be predicted that the $[F_3]^+$ cluster is more intense than the $[F_2]^+$ one and that in each cluster, the $[I_n]^+$ population is higher than the $[I_n\text{-}H_2]^+$ one. Furthermore, the population ratio between $[I_n]^+$ and $[I_n\text{-}H_2]^+$ should be similar. All this predictions are substantially confirmed by the experimental data; Figure 3 confirms the higher signals associated to the $[F_3]^+$ cluster and Table S-8 reports similar relative populations for $[I_n]^+$ and $[I_n\text{-}H_2]^+$ in the $[F_2]^+$ and $[F_3]^+$ clusters whereas $[I_2]^+$ and $[I_3]^+$ ions exhibit approximately a signal intensity twice than those of $[I_2\text{-}H_2]^+$ and $[I_3\text{-}H_2]^+$ ions, respectively.

Interestingly, the anomalous behavior of the $[F_4]^+$ cluster can be easily explained by the means of the computational results. In fact, $[I_4]^+$ and $[I_4\text{-}H_2]^+$ ions are likely produced from $[I_1]^+$ and from $[I_1\text{-}H_2]^+$, respectively. There is a much higher difference in reaction energies with a clear energy preference for the $[I_4\text{-}H_2]^+$ production than for $[I_4]^+$ (Table 2B). This easily explains the experimental predominance of the latter ion. From the above discussions, we can assign a large part of the fragmentations toward the $[F_2]^+$, $[F_3]^+$, and $[F_4]^+$ ion clusters to reactions which take place from $[I_1\text{-}H_2]^+$ and $[I_1\text{-}2H_2]^+$.

Table 2. **(A)** Computed dehydrogenation energies of $[I_n]^+$ ions for n=2, 3, and 4; **(B)** reaction energies for selected fragmentation routes of the tripodal $[GdQ+H]^+$ complex[a]

A

Ion	Fragmentation	ΔE^b (kcal/mol)
$[I_2]^+$	$[I_2]^+ \rightarrow [I_2\text{-}H_2]^+ + H_2$	+38.38
$[I_3]^+$	$[I_3]^+ \rightarrow [I_3\text{-}H_2]^+ + H_2$	+38.42
$[I_4]^+$	$[I_4]^+ \rightarrow [I_4\text{-}H_2]^+ + H_2$	+38.49

B

Produced Cluster	Process	ΔE^b (kcal/mol)
$[F_2]^+$	$[I_1\text{-}H_2]^+ \rightarrow [I_2]^+ + HCN$	+0.27
	$[I_1\text{-}2H_2]^+ \rightarrow [I_2\text{-}H_2]^+ + HCN$	+1.44
$[F_3]^+$	$[I_1\text{-}H_2]^+ \rightarrow [I_3]^+ + CH_3CN$	−5.38
	$[I_1\text{-}2H_2]^+ \rightarrow [I_3\text{-}H_2]^+ + CH_3CN$	−4.23
$[F_4]^+$	$[I_1]^+ \rightarrow [I_4]^+ + CH_3CH_2CN$	+2.24
	$[I_1\text{-}H_2]^+ \rightarrow [I_4\text{-}H_2]^+ + CH_3CH_2CN$	−4.49

[a]See Scheme 1 for details on the chemical structure of each product ions
[b]Electronic energies in the Born-Oppenheimer approximation. Complex ions energies are referred to the most stable isomer ($O_{ax}N_{eq}$-$O_{ax}N_{eq}$). See Tables S-10 up to S-17 plus Table S-19 for structural coordinates and energies

Conclusions

This study provides, for the first time, a detailed overview of MS behavior of a new tripodal quinolin-8-olate Gd complex investigated by IRMPD FTICR MS in the positive ion mode. The high mass accuracy and resolution provided by FTICR-MS allowed to unequivocally identify fragment ions derived by saturated and dehydrogenated product ions even when the isotopic distributions significantly overlap. The comparison of mass spectra after 100 ms IRMPD irradiation time with the ones obtained after 250 ms irradiation time allowed concluding that fragmentation of the precursor tripodal complex takes place in two distinct steps. The first one consists in the loss of the neutral 7-propenyl-8-hydroxyquinoline moiety with production of a four-coordinated positively-charged complex, which is responsible of a mass peak cluster labeled as $[F_1]^+$. Further irradiation induces additional fragmentation toward lighter positive complex ions whose presence has been evidenced by five additional cluster ions ($[F_n]^+$, n=2, 6). CID experiments performed on the $[F_1]^+$ cluster confirmed that it is the precursor of lighter fragments. Within this ion cluster, the high resolution of the FTICR MS allowed distinguishing three chemical species which differ in hydrogen content ($[I_1]^+$, $[I_1\text{-}H_2]^+$, and $[I_1\text{-}2H_2]^+$). Similarly, in the case of the $[F_2]^+$, $[F_3]^+$, and $[F_4]^+$ clusters, a hydrogenated and a dehydrogenated form (labeled as $[I_n]^+$ and $[I_n\text{-}H_2]^+$) have been detected and their relative populations have been quantified. Such relative populations are very similar in the $[F_2]^+$ and $[F_3]^+$ clusters, whereas a clear discontinuity has been detected in $[F_4]^+$. These findings have been used to give suggestions about the fragmentation pathways from $[F_1]^+$ to the lighter clusters. By comparing such experimental data with results from DFT computational studies, a fragmentation rationale has been suggested, which is able to explain the experimental findings. According to this picture, $[I_1\text{-}H_2]^+$ and $[I_1\text{-}2H_2]^+$ are the main responsible of the lighter fragments, which produce the $[F_2]^+$, $[F_3]^+$, and $[F_4]^+$ clusters. The observed relative populations of hydrogenated and dehydrogenated forms in each of the three clusters are in agreement with the computed reaction energies for the fragmentation processes. The $[F_5]^+$ cluster resulted from the overlap of two ions ($[I_5]^+$ and $[I_5\text{-}H]^+$), which differ for a single hydrogen atom content. Conversely, the $[F_6]^+$ cluster, originated from isotopologues associated with a single ionic specie.

Acknowledgment

This work was performed by using the instrumental facilities of CIGAS Center supported by EU (Project no. 2915/12), Regione Basilicata and Università degli Studi della Basilicata (USB). M.D.B. thanks USB for the university research fellowship, which allowed her to work in the field of 8-hydroxyquinoline hemicage ligands for metal complexation. This work was supported by Consortium INSTM through the PRISMA 2007 project.

References

1. Santos, L.S. (ed.): Reactive Intermediates: MS Investigations in Solution. Wiley-VCH, Weinheim (2010)
2. Dyson, P.J., Scott McIndoe, J.: Analysis of organometallic compounds using ion trap mass spectrometry. *Inorg. Chim. Acta* **354**, 68–74 (2003)
3. Qian, R., Guo, H., Liao, Y., Guo, Y., Ma, S.: Probing the mechanism of palladium-catalyzed addition of organoboronic acids to allenes in the presence of AcOH with ESI-FTMS. *Angew. Chem. Int. Ed.* **44**, 4771–4774 (2005)
4. Mosely, J.A., Murray, B.S., Parker, D.: Electron-capture dissociation and collision-induced dissociation of lanthanide metal-ligand complexes and lanthanide metal-ligand complexes bound to phosphopeptides. *Eur. J. Mass Spectrom.* **15**(2), 145–155 (2009)
5. Lau, R.L.C., Jiang, J., Ng, D.K.P., Chan, T.-W.D.: Fourier Transform ion cyclotron resonance studies of Lanthanide(III) porphyrin-phthalocyanineheteroleptic sandwich complexes using electrospray ionization. *J. Am. Soc. Mass Spectrom.* **8**, 161–169 (1997)
6. Godin, B., Tasciotti, E., Liu, X., Serda, R.E., Ferrari, M.: Multistage nanovectors: from concept to novel imaging contrast agents and therapeutics. *Acc. Chem. Res.* **18**, 979–989 (2011)
7. Henig, J., Tóth, E., Engelmann, J., Gottschalk, S., Mayer, H.A.: Macrocyclic Gd^{3+} chelates attached to a silsesquioxane core as potential magnetic resonance imaging contrast agents: synthesis, physicochemical characterization, and stability studies. *Inorg. Chem.* **49**, 6124–6138 (2010)
8. Soroka, K., Vithanage, R.S., Phillips, D.A., Walker, B., Dasgupta, P.K.: Fluorescence properties of metal complexes of 8-hydroxyquinoline-5-sulfonic acid and chromatographic applications. *Anal. Chem.* **59**, 629–636 (1987)
9. Hollingshead, R.G.W.: Oxine and Its Derivatives, vol. I-IV. Butterworths, London (1954–1956)
10. Phillips, J.P.: The reactions of 8-quinolinol. *Chem. Rev.* **56**, 271–297 (1956)
11. Hollingshead, R.G.W.: Studies on oxine and its derivatives: the sensitivity and selectivity of some 7-substituted 8-hydroxyquinoline-5-sulphonic acids and some 2-substituted 8-hydroxyquinoline-4-carboxylic acids towards certain metals. *Anal. Chim. Acta* **19**, 447–457 (1958)
12. Dowlings, S.D., Seitz, W.R.: Effect of metal–ligand ratio on polarization of fluorescence from metal-8-quinolinol complexes. *Spectrochim. Acta Part A: Mol. Spectrosc.* **40**, 991–993 (1984)
13. Fernandez-Gutierrez, A., Munoz de la Pena, A.: In: Schulman, S.G. (ed.) Molecular luminescence spectroscopy. Methods and Application, Part I, pp. 371–546. Wiley, New York (1985)
14. Farruggia, G., Iotti, S., Prodi, L., Montalti, M., Zaccheroni, N., Savage, P.B., Trapani, V., Sale, P., Wolf, F.I.: 8-hydroxyquinoline derivatives as fluorescent sensors for magnesium in living cells. *J. Am. Chem. Soc.* **128**, 344–350 (2006)
15. Bardez, E., Devol, I., Larrey, B., Valeur, B.: Excited State Processes in 8-hydroxyquinoline: photoinduced tautomerization and solvation effects. *J. Phys. Chem. B* **101**, 7786–7793 (1997)
16. Amati, M., Belviso, S., Cristinziano, P., Minichino, C., Lelj, F., Aiello, I., La Deda, M., Ghedini, M.: 8-Hydroxyquinoline monomer, water adducts, and dimer. Environmental influences on structure, spectroscopic properties, and relative stability of cis and trans conformers. *J. Phys. Chem.* **111**, 13403–13414 (2007)
17. Tang, C.W., VanSlyke, S.A.: Organic electroluminescent diodes. *Appl. Phys. Lett.* **51**, 913–915 (1987)
18. Zhigang, L., Hong, M.: Organic Light-EmittingMaterials and Devices, Chap. 3. Boca Raton, CRC Press: Taylor and Francis Group (2007)
19. Amati, M., Lelj, F.: Luminescent compounds *fac*- and *mer*-aluminum tris(quinolin-8-olate). A pure and hybrid density functional theory and time-dependent density functional theory investigation of their electronic and spectroscopic properties. *J. Phys. Chem. A* **107**, 2560–2569 (2003)
20. Tallec, G., Imbert, D., Fries, P.H., Mazzanti, M.: Highly stable and soluble bis-aqua Gd, Nd. Yb complexes as potential bimodal MRI/NIR Imaging Agents. *Dalton Trans.* **39**, 9490–9492 (2010)

21. Eliseevaa, S.V., Bünzli, J.-C.G.: Lanthanide luminescence for functional materials and bio-sciences. *Chem. Soc. Rev.* **39**, 189–227 (2010)
22. Marshall, A.G., Hendrickson, C.L., Jackson, G.S.: Fourier transform ion cyclotron resonance mass spectrometry: a primer. *Mass Spectrom. Rev.* **17**, 1–35 (1998)
23. Marshall, A.G.: Milestones in Fourier transform ion cyclotron resonance mass spectrometry technique development. *Int. J. Mass Spectrom.* **200**, 331–356 (2000)
24. Gauthier, J.W., Trautman, T.R., Jacobson, D.B.: Sustained off-resonance irradiation for collision-activated dissociation involving Fourier transform mass spectrometry. Collision-activated dissociation technique that emulates infrared multiphoton dissociation. *Anal. Chim. Acta* **246**, 211–225 (1991)
25. Woodlin, R.L., Bomse, D.S., Beauchamp, J.L.: Multiphoton dissociation of molecules with low power continuous wave infrared laser radiation. *J. Am. Chem. Soc.* **100**, 3248–3250 (1978)
26. Little, D.P., Speir, J.P., Senko, M.W., O'Connor, P.B., McLafferty, F.W.: Infrared multiphoton dissociation of large multiply-charged ions for biomolecule sequencing. *Anal. Chem.* **66**, 2809–2815 (1994)
27. Dunbar, R.C., McMahon, T.B.: Activation of unimolecular reactions by ambient blackbody radiation. *Science* **279**, 194–197 (1998)
28. Price, W.D., Schnier, P.D., Williams, E.R.: Tandem mass spectrometry of large biomolecule ions by blackbody infrared radiative dissociation. *Anal. Chem.* **68**, 859–866 (1996)
29. McCormack, A.L., Jones, J.L., Wysocki, V.H.: Surface-induced dissociation of multiply protonated peptides. *J. Am. Soc. Mass Spectrom.* **3**, 859–862 (1992)
30. Chorush, R.A., Little, D.P., Beu, S.C., Wood, T.D., McLafferty, F.W.: Surface induced dissociation of multiply protonated proteins. *Anal. Chem.* **67**, 1042–1046 (1995)
31. Cooper, H.J., Hakansson, K., Marshall, A.G.: The role of electron capture dissociation in biomolecular analysis. *Mass Spectrom. Rev.* **24**, 201–222 (2005)
32. Chrisman, P.A., Pitteri, S.J., McLuckey, S.A.: Parallel ion parking: improving conversion of parents to first-generation products in electron transfer dissociation. *Anal. Chem.* **77**, 3411–3414 (2005)
33. Sleno, L., Volmer, D.A.: Ion activation methods for tandem mass spectrometry. *J. Mass Spectrom.* **39**, 1091–1112 (2004)
34. Laskin, J., Futrell, J.H.: Activation of large ions in FT-ICR mass spectrometry. *Mass Spectrom. Rev.* **24**, 135–167 (2005)
35. Cooper, H.J., March, R.E., Todd, J.F.J.: Practical aspects of ion trap mass spectrometry. Vol. V, Applications to ion trapping devices. CRC Press, Boca Raton (2010)
36. McFarland, M.A., Marshall, A.G., Hendrickson, C.L., Nilsson, C.L.: Structural characterization of the gm1 ganglioside by infrared multiphoton dissociation, electron capture dissociation, and electron detachment dissociation electrospray ionization FT-ICR MS/MS. *J. Am. Soc. Mass Spectrom.* **16**, 752–762 (2005)
37. Polfer, N.C.: Infrared multiple photon dissociation spectroscopy of trapped ions. *Chem. Soc. Rev.* **40**, 2211–2221 (2011)
38. Bianco, G., Labella, C., Pepe, A., Cataldi, T.R.I.: Scrambling of autoinducing precursor peptides investigated by infrared multiphoton dissociation with electrospray ionization and Fourier-transform ion cyclotron resonance mass spectrometry. *Anal. Bioanal. Chem.* **405**(5), 1721–1732 (2013)
39. Cataldi, T.R.I., Ricciardi, G., Bianco, G., Pietrangeli, D., Abate, S.: Mass spectrometric evidence for collisionally induced removal of H(2) from monoanions of (10)B nido-carborane derivatives investigated by electrospray ionization quadrupole linear ion trap and Fourier transform ion cyclotron resonance mass spectrometry. *Rapid Commun. Mass Spectrom.* **23**, 1927–1933 (2009)
40. Zhao, Y., Truhlar, D.G.: The M06 suite of density functionals for main group thermochemistry, thermochemical kinetics, noncovalent interactions, excited states, and transition elements: two new functionals and systematic testing of four M06-class functionals and 12 other functional. *Theor. Chem. Acc.* **120**, 215–241 (2008)
41. Frisch, M.J., Trucks, G.W., Schlegel, H.B., Scuseria, G.E., Robb, M.A., Cheeseman, J.R., Scalmani, G., Barone, V., Mennucci, B., Petersson, G.A., Nakatsuji, H., Caricato, M., Li, X., Hratchian, H.P., Izmaylov, A.F., Bloino, J., Zheng, G., Sonnenberg, J.L., Hada, M., Ehara, M., Toyota, K., Fukuda, R., Hasegawa, J., Ishida, M., Nakajima, T., Honda, Y., Kitao, O., Nakai, H., Vreven, T., Montgomery Jr., J.A., Peralta, J.E., Ogliaro, F., Bearpark, M., Heyd, J.J., Brothers, E., Kudin, K.N., Staroverov, V.N., Kobayashi, R., Normand, J., Raghavachari, K., Rendell, A., Burant, J.C., Iyengar, S.S., Tomasi, J., Cossi, M., Rega, N., Millam, N.J., Klene, M., Knox, J.E., Cross, J.B., Bakken, V., Adamo, C., Jaramillo, J., Gomperts, R., Stratmann, R.E., Yazyev, O., Austin, A.J., Cammi, R., Pomelli, C., Ochterski, J.W., Martin, R.L., Morokuma, K., Zakrzewski, V.G., Voth, G.A., Salvador, P., Dannenberg, J.J., Dapprich, S., Daniels, A.D., Farkas, Ö., Foresman, J.B., Ortiz, J.V., Cioslowski, J., Fox, D.J.: Gaussian 09, Revision A.1. Gaussian, Inc, Wallingford CT (2009)
42. Ditchfield, R., Hehre, W.J., Pople, J.A.: Self-consistent molecular orbital methods. 9. Extended Gaussian-type basis for molecular-orbital studies of organic molecules. *J. Chem. Phys.* **54**, 724–728 (1971)
43. Hehre, W.J., Ditchfield, R., Pople, J.A.: Self-consistent molecular orbital methods. 1. Use of Gaussian expansions of Slater-type atomic orbitals. *J. Chem. Phys.* **56**, 2257–2261 (1972)
44. Hariharan, P.C., Pople, J.A.: Accuracy of AH equilibrium geometries by single determinant molecular-orbital theory. *Mol. Phys.* **27**, 209–214 (1974)
45. Gordon, M.S.: The isomers of silacyclopropane. *Chem. Phys. Lett.* **76**, 163–168 (1980)
46. Hariharan, P.C., Pople, J.A.: Influence of polarization functions on molecular-orbital hydrogenation energies. *Theo. Chim. Acta* **28**, 213–222 (1973)
47. Nicklass, A., Dolg, M., Stoll, H., Preuss, H.: Ab initio energy-adjusted pseudopotentials for the noble gases Ne through Xe: calculation of atomic dipole and quadrupole polarizabilities. *J. Chem. Phys.* **102**, 8942–8952 (1995)
48. Bacskay, G.B.A.: Quadratically convergent Hartree-Fock (QC-SCF) method. Application to closed systems. *Chem. Phys.* **61**, 385–404 (1981)
49. Fluckiger, P., Luthi, H.P., Portmann, S., Weber, J.: MOLEKEL 4.3. Swiss Center for Scientific Computing, Manno (2000–2002)
50. Portmann, S., Luthi, H.P.: MOLEKEL: an interactive molecular graphic tool. *Chimia* **54**, 766–770 (2000)
51. De Bonis, M., Lelj, F. et al. manuscript in preparation.
52. Wang, J., Oyler, K.D., Bernhard, S.: Synthesis and characterization of hemicaged 8-hydroxyquinoline chelates with enhanced electrochemical and photophysical properties. *Inorg. Chem.* **46**, 5700–5706 (2007)
53. Evans, D. F.: Determination of the paramagnetic susceptibility of substances in solution by nuclear magnetic resonance. *J. Chem. Soc.* 2003–2005 (1959). doi:10.1039/JR9590002003
54. Dickinson, W.C.: The time average magnetic field at the nucleus in nuclear magnetic resonance experiments. *Phys. Rev.* **81**, 717–731 (1951)
55. Bain, A.G., Berry, J.F.: Diamagnetic Corrections and Pascal's Constants. *J. Chem. Ed.* **85**, 532–535 (2008)
56. Weber, R.J.M., Southam, A.D., Sommer, U., Viant, M.R.: Characterization of isotopic abundance measurements in high resolution FT-ICR and Orbitrap mass spectra for improved confidence of metabolite identification. *Anal. Chem.* **83**, 3737–3743 (2011)
57. do Lago, C.L., Kascheres, C.: New method of isotope pattern analysis. *Comput. Chem.* **15**, 149–155 (1991)
58. Rosman, K.J.R., Taylor, P.D.P.: Isotopic compositions of the elements 1997 (Technical Report). *Pure Appl. Chem.* **70**, 217–235 (1998)
59. Henderson, W., Scott McIndoe, J.S.: The ESI MS behavior of main group organometallic compounds. Mass spectrometry of inorganic, coordination, and organometallic compounds, Chap 6. John Wiley, Chichester (2005)
60. Audi, G., Wapstra, A.H.: The 1995 update to the atomic mass evaluation. *Nucl. Phys. A* **595**, 409–480 (1995)
61. Purcell, K. F., Kotz, J. C. In: Inorganic Chemistry, Chap 10. International Edition Holt-Saunders, Japan (1985)
62. Sun, L.-N., Zhang, H.-J., Yu, J.-B., Yu, S.-Y., Peng, C.-Y., Dang, S., Guo, X.-M., Feng, J.: Near-Infrared emission from novel tris(8-hydroxyquinolinate)lanthanide(III) Complexes-functionalized Mesoporous SBA-15. *Langmuir* **24**, 5500–5507 (2008)
63. Bertini, I., Luchinat, C.: NMR of paramagnetic substances. *Coord. Chem. Rev.* **150**, 1–300 (1996)